FINAL REPORT

for

July 18, 2006 – July 31, 2007

of

Hybrid Coarse Mesh Transport/Diffusion Method for PBR Neutronics Analysis

Submitted by

Farzad Rahnema (PI) and Dingkang Zhang

Georgia Institute of Technology

in Collaboration with
Idaho National Laboratory

July 30, 2007

Summary

The objective of this project is to develop a method to generate transport theory response functions for non-multiplying regions in cylindrical geometry typical of pebble bed reactors (PBRs). This was accomplished in the three numerical steps. In the first step, the predefined phase space distribution of neutron particles on the boundary of a coarse mesh was first expanded as a multi-product of a set of orthogonal basis functions. In the second step, response functions for each cylindrical coarse mesh were generated by solving each local fixed source problem with the boundary condition imposed on one of the bounding surfaces. In the last step, a consistency check was performed to verify its accuracy.

In this project, the response expansion method was implemented into the MCNP code to calculate the response functions for coarse meshes in the inner and outer reflectors. The results obtained as a superposition of response functions were compared with the continuous energy Monte Carlo reference calculations. The excellent agreement between the two calculations indicates that the response functions can reproduce the reference solutions.

I. Introduction

The current generation of core neutronics methods for an analysis of the pebble bed reactor (PBR) is based on nodal diffusion theory and utilizes homogenized cross sections and other physics data generated by single assembly, infinite medium transport theory calculations. One of the primary limitations of nodal diffusion theory is its inadequacy to treat regions in the vicinity of strong neutron absorbers. A prime example of this shortcoming is the controlled reflector region in PBRs. These regions with no neutron multiplication and strong absorption do not receive satisfactory treatment in the nodal diffusion model. The goal of this project is to develop a method to generate the response functions for these regions. The response functions can be accommodated into the nodal diffusion equation to provide a transport solution for regions where the diffusion approximation is not sufficient.

The project consists of two phases. Phase I contains the development of 2-D work. Phase II was originally planed to further extend the method to 3-D. Because of funding unavailability, phase II has not been funded by INL. However, as requested by INL, we have generated homogenized cross sections for a simplified 1D slab PRB problem in phase II.

This final report is divided into four major sections. Section II contains an overview summarizing the objectives and work scope. Section III contains a complete description of the work performed in this project. Finally, Section IV highlights the project accomplishments.

II. Project Overview

Objective

The objective of this project is to develop a method to generate transport theory response functions for non-multiplying regions in 2-D cylindrical geometry typical of pebble bed reactors (PBRs). The method is to be implemented into the MCNP code to obtain a local transport solution for each unique coarse mesh in the outer or inner region as a response to incoming neutrons impinging on one of the bounding surfaces.

Work Scope

The main scope of work involves the development of expansion functions in 2D cylindrical geometry, the implementation of the new expansion functions into the MCNP code, the generation of response functions for non-multiplying regions, the consistency check to show the accuracy of the response functions, and generation of homogenized cross sections for a simplified 1-D slab PBR problem. The project consists of two phases. The phase I effort was focused on generation of the response functions for coarse meshes in the inner or outer reflector. The phase II effort was focused on generation of homogenized cross sections to account for intra-nodal leakages.

III. Technical Narrative

Task 1 Extend the method of calculating coarse mesh response functions from 1-D slab geometry to 2-D cylindrical geometry

Task Summary

The aim of this task was to extend the method of calculating the response functions from 1-D coarse meshes to 2-D cylindrical coarse meshes in both inner and outer reflectors. The main requirement is that this method can provide the response functions, in terms of node-averaged flux, surface-averaged flux and outgoing partial currents, corresponding to the incoming flux entering from one of the bounding surfaces.

Work Performed

The coarse-mesh methodology for the transport treatment of a set of selected nodes has been tailored to match the requirements of the CMFD method developed by INL and described in the proposal. INL method integrates the response matrices for the nodes necessitating transport treatment transparently in its formulation. As a result, Georgia Tech provides INL with response matrices that contain node responses to unit incoming partial currents, both in terms of node surface fluxes and node partial outgoing currents. The latter are needed to couple the transport-treated node to its neighbors.

Figure 1 illustrates the schematic configuration of a 2D PBMR400 pebble bed reactor, consisting of an inner reflector region, an annular fuel region and a controlled outer reflector. Let's begin with dividing both the outer and inner reflectors into a number of coarse meshes. The response functions of the coarse mesh corresponding to an incoming current from one of the adjacent regions can be calculated by solving the local problem below.

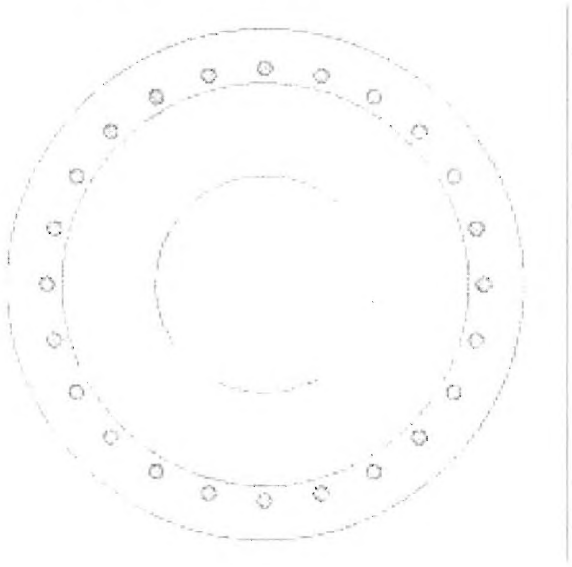

Fig. 1: 2-D simplified PBMR400 model

$$\frac{\mu}{r}\frac{\partial}{\partial r}\left(r\psi_l\left(r,\theta,\hat{\Omega},E\right)\right)+\frac{\eta}{r}\frac{\partial}{\partial\theta}\psi_l\left(r,\theta,\hat{\Omega},E\right)-\frac{1}{r}\frac{\partial}{\partial\omega}\left(\eta\psi_l\left(r,\theta,\hat{\Omega},E\right)\right)$$
$$+\sigma_t\left(r,\theta,E\right)\psi_l\left(r,\theta,\hat{\Omega},E\right)=Q_l\left(r,\theta,\hat{\Omega},E\right)+\int_0^\infty dE'\int_{4\pi}d\Omega'\ \sigma_s\left(r,\theta,\hat{\Omega}',E'\to\hat{\Omega},E\right)\psi_l\left(r,\theta,\hat{\Omega}',E'\right) \quad (1)$$

with the following boundary condition

$$\psi_i^-\left(r_{ij},\theta_{ij},\hat{\Omega},E\right)=\psi_j^+\left(r_{ij},\theta_{ij},\hat{\Omega},E\right) \text{ where } (r_{ij},\theta_{ij})\in\left\{V_i\cap V_j\right\} \text{ for all } V_j \text{ bounding } V_i \quad (2)$$

In the above equations, $\psi_i\left(r,\theta,\hat{\Omega},E\right)$ is the neutron angular flux within coarse mesh i, r and θ are spatial variables in the cylindrical coordinate, ω and ξ are angular variables. Q is the internal volumetric source that may also include scattering neutrons. V_i represents all the sub-volume elements (i.e. coarse meshes). The superscripts "+" and "-"on the angular flux indicate the outgoing and incoming direction, respectively.

The MCNP code has been adapted to yield the solution to the local problem of Eq. (1). In the source-sampling subroutine, the initial position, direction and energy of source neutrons are sampled based on the predefined phase-space distribution on the boundary of a coarse mesh. If $f(r,\theta,\hat{\Omega},E)$ is the predefined distribution function, the initial position, energy and direction of incoming neutrons are sampled from the following distribution.

$$\Gamma_{ij}^-(w_{ts}^-)=f\left(r,\theta,\hat{\Omega},E\right) \quad (3)$$

In the tally subroutine, the expected value of response functions, in terms of the node-average flux, surface-averaged flux and partial currents crossing a coarse mesh, are tallied as the probability that initial neutrons and their progenies escape from the coarse mesh through a specific surface, scaled by a weight factor determined by the orders of the expansion and the location, energy and direction of the exiting neutrons.

$$RJ(k)_{i,j'\to j}^{n'\to n}=\frac{1}{NA_{ij}^n}\sum_{c=1}^{N}f_{ij}^{+,n}\left(\vec{r}_c,E_c,\hat{\Omega}_c\right)w_c \quad (4)$$

where $\vec{r}_c,E_c,\hat{\Omega}_c$ and w_c are the position, energy, direction and weight of the exiting neutrons, and $f_{ij}^{+,n}\left(\vec{r}_c,E_c,\hat{\Omega}_c\right)$ are the expansion functions.

The code was tested by comparisons with results from direct MCNP simulations on 2-D benchmark problems. A consistency check to further verify the accuracy of the response functions, based on comparisons of the superposition of response functions and MCNP solutions, was performed upon the completion of task 2.

Task 2 Development of 2D cylindrical expansion functions

Task Summary

The aim of this task was to develop an expansion scheme to approximate the angular flux on a coarse mesh interface in 2D cylindrical geometry. The idea behind expansion functions is the development of the boundary condition imposed on the node boundary as an expansion of an orthogonal set of basis functions in space, energy and angle. The basis functions are selected so that a relatively low order truncation would lead to accurate solutions inside the node. The Monte Carlo code MCNP allows surface-source boundary conditions in terms of isotropic and cosine angular distributions and uniform and linear spatial distribution. Higher orders of expansion would require a modification to the MCNP source code. The expansion approximation should guarantee conservation of particle and be able to provide the scalar flux at the incident surface.

Work Performed

(1) Expansion functions

Following Mosher and Rahnema (2006)[1] and Forget and Rahnema (2007)[2], one may expand the angular current at each interface in terms of Legendre polynomials as in Eq. (5). This is a natural choice, since the 0^{th} order expansion in angle corresponds to an isotropic surface source, and the 0^{th} order expansion in space corresponds to a uniform source. However, this expansion scheme cannot be applied to cylindrical geometry as in this project, since an isotropic angular current (i.e. angular flux $\Psi = 1/\mu$), leads to an infinite scalar flux on the incident surface.

$$J(x,\mu,\phi,E) = \sum_{i,j,k,l} J_{ijkl} P_i(x) P_i(\mu) P_k(\phi) P_l(E) \tag{5}$$

To accomplish the goals of this task, we choose to expand the angular flux, instead of angular current, at each surface in terms of a set of expansion (basis) functions.

$$\psi(x,\hat{\Omega},E) = \sum_{i,j,k,l} c_{ijkl} f_{ijkl}(x,\hat{\Omega},E) \tag{6}$$

In the above equation, c_{ijkl} are expansion coefficients, and $f_{ijkl}(x,\hat{\Omega},E)$ represent expansion functions. However, in order to ensure that the total number of particles (or current) is conserved, the expansion functions must be constructed to have the following orthogonality.

$$\int dx \int dE \int_{\vec{n}\cdot\hat{\Omega}>0} d\hat{\Omega}(\vec{n}\cdot\hat{\Omega}) f_{ijkl}(x,\hat{\Omega},E) f_{i'j'k'l'}(x,\hat{\Omega},E) = A_{ijkl}\delta_{ii'}\delta_{jj'}\delta_{kk'}\delta_{ll'} \tag{7}$$

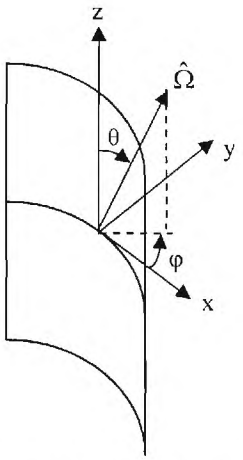

Fig. 2: Angular variables in a 2D cylindrical surface

As an example, take a 2D cylindrical surface shown in Fig. 2 in which axis z is chosen to be parallel with the axis of the cylinder and y represents the normal direction at point $\vec{r}$. In this case, the expansion functions can be written as in the following form[3].

---

[1] Scott Mosher and F. Rahnema, "The Incident Flux Response Expansion Method for Heterogeneous Coarse Mesh Transport Problems," *Transport Theory and Statistical Physics*, **34**, No. 6, 1-26 (2006).

[2] Benoit Forget and Farzad Rahnema, "Hybrid Coarse Mesh Radiation Transport Method for Whole Core Reactor Criticality Analysis," *Nucl. Sci. Eng.*, Submitted (December 2006).

[3] Dingkang Zhang, Farzad Rahnema, and Abderrafi M Ougouag, "New Expansion Functions for Calculation of Coarse Mesh Response Functions", the 2007 ANS Annual Meeting, Boston, MA, June 24-28, 2007

$$f_{ijkl}\left(x,\hat{\Omega},E\right)=\overline{P}_i\left[x_{\min},x_{\max}\right](x)U_j\left(\cos\theta\right)P_j\left(\cos\phi\right)\overline{P}_l\left[E_{g-1},E_g\right](E) \tag{8}$$

where scaled Legendre polynomials $\overline{P}_i\left[x_{\min},x_{\max}\right](x)$ and Chebyshev polynomials of the second kind $U_j(x)$ are defined as:

$$\overline{P}_i\left[x_{\min},x_{\max}\right](x)=P_i\left(\frac{2\left(x-x_{\min}\right)}{x_{\max}-x_{\min}}-1\right) \tag{9}$$

and

$$\begin{aligned} U_0(x)&=1 \\ U_1(x)&=2x \\ U_n(x)&=2xU_{n-1}(x)-U_{n-2}(x) \quad \text{for } n\geq 2 \end{aligned} \tag{10}$$

(2) Consistency check

The method and expansion functions developed in tasks 1 and 2 have been successfully implemented into the MCNP code. Generation of response functions consists of two steps. In the first step, the MCNP code was used to compute a reference solution, and the actual neutron spatial, energy and angular distributions were tallied and expanded in terms of the expansion functions constructed in this research. In the second step, the response functions of a coarse mesh associated with the incoming neutron flux at each bounding surface were generated.

To verify the validity of the method, a 2D cylindrical benchmark problem shown in Fig. 3 was considered. The 2-D benchmark consists of an inner reflector region with a diameter of 2 meters (m), an annular fuel region of 0.85 m thickness and a 0.5 m thick controlled outer reflector region. There are 24 control rods each of 13 cm diameter whose centers are positioned on the circumference of 3.974 m diameter ring. The material compositions are listed in Table 1.

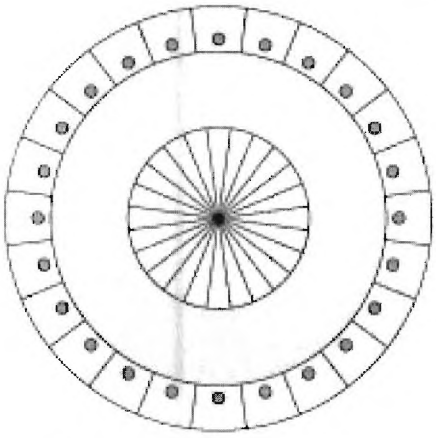

Fig. 3: Geometric configuration of a 2D cylindrical benchmark problem

Table 1 Material composition in each region

Region	Material	Atomic Density (10^{-24})
Inner Reflector	C	1.18234E-01
	U234	1.16811E-07
	U235	1.19359E-05

Fuel	U238	1.10859E-04
	Xe135	3.43000E-11
	O16	2.45830E-04
	Si	2.75487E-04
	Ni	1.04518E-04
	Cr	1.34381E-04
	Fe	5.07660E-04
	C	6.81785E-02
Outer Reflector	C	1.18894E-01
Control Rod	B10	3.20000E-06
	C	9.54760E-02

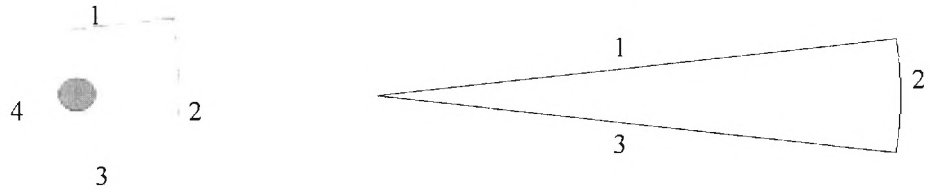

(a) coarse mesh in the outer reflector (b) coarse mesh in the inner reflector

Fig. 4: Configurations of coarse meshes

Both the outer and inner reflectors were divided into 24 coarse meshes. The geometrical configurations of these coarse meshes are shown in Figs. 4. The response functions, in terms of exiting partial currents, surface-averaged angular fluxes and node-averaged fluxes, are listed in Tables A1-A4.

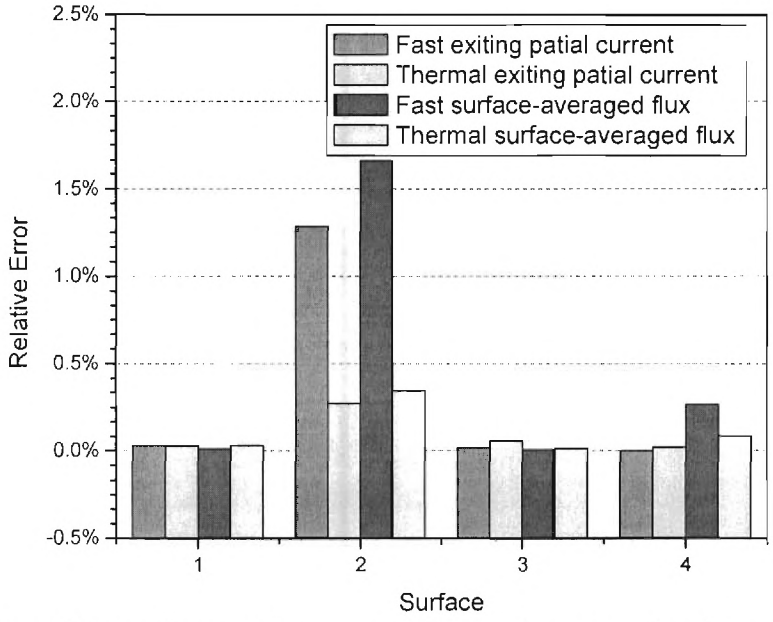

Fig. 5: Relative difference between the superposition based response functions and reference solutions for the outer reflector coarse mesh

To check the accuracy of these response functions, the superposition of these response functions was compared with the reference results computed from the continuous-energy MCNP simulations. The relative difference between the two solutions for the outer reflector coarse mesh is illustrated in Fig. 5. The detailed comparisons for both the inner and outer reflector coarse meshes are listed in Tables A5-A8. It can be found that the agreement between the two solutions is excellent. Most of the relative errors are less than 0.2%. The maximum relative difference of 1.6% occurs on the outer surface (surface 2 in Fig. 4) of the coarse mesh in the outer reflector where the uncertainty of the reference solution is about 1%; however it is still within the two standard deviations of the reference solutions. These results indicate that the response functions based on the method and expansion functions developed in this work are accurate and can reproduce solutions to the same level as continuous energy MCNP calculations.

Task 3 Generation of homogenized cross sections for a 1-D slab problem specified by INL

Task summary:

The aim of the task was to generate homogenized parameters (cross sections, discontinuity factors) for 1-D coarse meshes. Conventionally, the assumption of infinite media (i.e. specular reflection boundary condition) is used to calculate approximate spectrum for each coarse mesh (lattice cell) and then homogenized data are collapsed. To account for the intra-nodal leakage, the ratios of incoming/outgoing partial currents provided by INL were taken into account when we calculated the homogenized parameters.

Work performed

The problem is a 1-D adaptation of a realistic 2-D model of the PBMR400 pebble bed reactor shown in Fig. 3. The specifications for the 2-D model are based on data provided by INL and are representative of an equilibrium core. The 1-D benchmark is a section of the 2-D configuration taken along a semi-plane perpendicular to the paper and passing through the centers of the reactor and of one of the control rods. Its geometrical layout and its subdivision into nodes are illustrated in Figure 6. Reflective and vacuum boundary conditions were imposed on the left and right boundary of the system, respectively. The width of each region was taken to be the same as the corresponding radial width of the 2-D region. Material densities in each region are listed in Table 2. The ratios of incoming/outgoing partial currents provided by INL are illustrated in Table A9 in Appendix

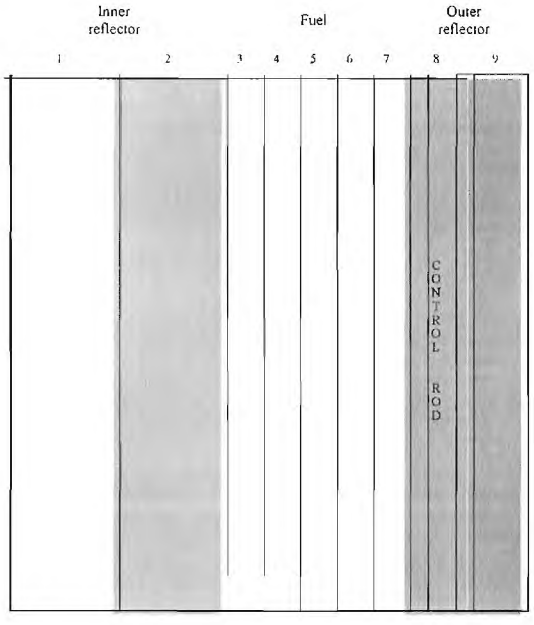

Fig. 6: 1-D simplified PBMR400 models

Table 2: Material compositions in each region (unit: 10E24 atoms/cm^{-3})

Elements	Inner reflector	Fuel	Outer reflector	Control Rod
C	1.18234E-01	6.81785E-02	1.18894E-01	9.54760E-02
U-234		1.16811E-07		
U-235		1.19359E-05		
U-238		1.10859E-04		
Xe-135		3.43000E-11		
O		2.45830E-04		
Si		2.75487E-04		
Ni		1.04518E-04		
Cr		1.34381E-04		
Fe		5.07660E-04		
B				3.20000E-06

A continuous energy Monte Carlo calculation was performed to calculate the neutron angular flux $\psi(z,\mu,E)$ within each coarse mesh. To preserve various reaction rates, the homogenized multi-group cross section were computed by the following equations:

$$\sigma_g = \frac{\int_V dz \int_{E_{g-1}}^{E_g} dE \int_{-1}^{1} d\mu \psi(z,\mu,E)\sigma(z,E)}{\int_V dz \int_{E_{g-1}}^{E_g} dE \int_{-1}^{1} d\mu \psi(z,\mu,E)}$$

$$\sigma_{a,g} = \frac{\int_V dz \int_{E_{g-1}}^{E_g} dE \int_{-1}^{1} d\mu \psi(z,\mu,E)\sigma_a(z,E)}{\int_V dz \int_{E_{g-1}}^{E_g} dE \int_{-1}^{1} d\mu \psi(z,\mu,E)}$$

$$\sigma_{f,g} = \frac{\int_V dz \int_{E_{g-1}}^{E_g} dE \int_{-1}^{1} d\mu \psi(z,\mu,E)\sigma_f(z,E)}{\int_V dz \int_{E_{g-1}}^{E_g} dE \int_{-1}^{1} d\mu \psi(z,\mu,E)}$$

$$\nu\sigma_{f,g} = \frac{\int_V dz \int_{E_{g-1}}^{E_g} dE \int_{-1}^{1} d\mu \psi(z,\mu,E)\nu\sigma_f(z,E)}{\int_V dz \int_{E_{g-1}}^{E_g} dE \int_{-1}^{1} d\mu \psi(z,\mu,E)}$$

$$\sigma_s^{g'g} = \frac{\int_V dz \int_{E_{g-1}}^{E_g} dE \int_{E_{g'-1}}^{E_{g'}} dE' \int_{-1}^{1} d\mu' \int_{-1}^{1} d\mu \psi(z,\mu',E') \nu\sigma_s(z,E' \to E,\mu_0)}{\int_V dz \int_{E_{g-1}}^{E_g} dE \int_{-1}^{1} d\mu \psi(z,\mu,E)}$$

Table A10 shows the MCNP collapsed two-group cross sections as well as discontinuity factors for nodes 1-9.

IV. Summary and Conclusions

Milestone/Task Description	Planned Completion Date	Actual Completion Date	Percent Complete
Task 1: 2D extension	October 17, 2006	October 17, 2006	100%
Task 2: 2D representation functions	December 17, 2006	December 17, 2006	100%
Task 3: Cross section generation	June 30, 2007	June 30, 2007	100%

We have successfully extended the method of calculating coarse mesh response functions from 1D slab to 2D cylindrical geometry. A set of new expansion functions, has been developed and implemented into the MCNP code. Unlike the Legendre expansion functions, the new expansion set avoids scalar flux singularity on the incident surface and at the same time ensures conservation of particles, i.e. the total current crossing an interface remains unchanged after expansion. A consistency check has been performed to demonstrate the accuracy of the method and the expansion functions. In addition, the MCNP code has been used to generate the homogenized parameters for the simplified 1-D PBR problem to account for intra-nodal leakages.

IV. APPENDIX:

Table A1: Response function of the coarse mesh in the outer reflector, in terms of exiting currents

Incoming surface	Group	Exiting Currents at outgoing surfaces							
		1		2		3		4	
		Fast	Thermal	Fast	Thermal	Fast	Thermal	Fast	Thermal
1	Fast	6.166E-01	1.086E-01	1.836E-03	1.297E-02	1.988E-04	5.156E-03	1.896E-01	4.813E-02
	Thermal	6.645E-07	8.251E-01	0.000E+00	3.513E-02	0.000E+00	5.127E-03	1.920E-07	1.051E-01
2	Fast	0.000E+00	0.000E+00	0.000E+00	0.000E+00	0.000E+00	0.000E+00	0.000E+00	0.000E+00
	Thermal	0.000E+00	0.000E+00	0.000E+00	0.000E+00	0.000E+00	0.000E+00	0.000E+00	0.000E+00
3	Fast	1.949E-04	5.166E-03	1.840E-03	1.296E-02	6.165E-01	1.087E-01	1.896E-01	4.815E-02
	Thermal	0.000E+00	5.128E-03	0.000E+00	3.516E-02	6.778E-07	8.251E-01	1.131E-07	1.051E-01
4	Fast	6.605E-02	3.002E-02	9.495E-04	1.382E-02	6.604E-02	3.001E-02	6.733E-01	9.294E-02
	Thermal	3.491E-07	7.713E-02	0.000E+00	8.394E-03	2.659E-07	7.710E-02	1.909E-06	7.921E-01

Table A2: Response function of the coarse mesh in the outer reflector, in terms of surface and node averaged fluxes

Incoming surface	Group	Surface-averaged flux at outgoing surfaces								Node-averaged flux	
		1		2		3		4			
		Fast	Thermal	Fast	Thermal	Fast	Thermal	Fast	Thermal	Fast	Thermal
1	Fast	3.309E+00	1.973E-01	3.156E-03	2.246E-02	3.408E-04	8.929E-03	3.680E-01	8.424E-02	1.979E+01	2.178E+01
	Thermal	2.132E-06	3.686E+00	0.000E+00	6.092E-02	0.000E+00	8.830E-03	2.957E-07	1.911E-01	1.361E-05	4.636E+01
2	Fast	0.000E+00	0.000E+00	0.000E+00	0.000E+00	0.000E+00	0.000E+00	0.000E+00	0.000E+00	0.000E+00	0.000E+00
	Thermal	0.000E+00	0.000E+00	0.000E+00	0.000E+00	0.000E+00	0.000E+00	0.000E+00	0.000E+00	0.000E+00	0.000E+00
3	Fast	3.289E-04	8.967E-03	3.150E-03	2.242E-02	3.309E+00	1.974E-01	3.680E-01	8.429E-02	1.976E+01	2.176E+01
	Thermal	0.000E+00	8.839E-03	0.000E+00	6.107E-02	2.723E-06	3.685E+00	1.349E-07	1.909E-01	1.294E-05	4.637E+01
4	Fast	1.234E-01	5.217E-02	1.609E-03	2.397E-02	1.232E-01	5.226E-02	3.365E+00	1.672E-01	2.856E+01	2.684E+01
	Thermal	9.444E-07	1.402E-01	0.000E+00	1.446E-02	3.912E-07	1.404E-01	7.587E-06	3.644E+00	4.370E-05	4.227E+01

Table A3: Response function of the coarse mesh in the inner reflector, in terms of exiting currents

Incoming surface	Group	Exiting Currents at outgoing surfaces					
		1		2		3	
		Fast	Thermal	Fast	Thermal	Fast	Thermal
1	Fast	6.202E-01	9.987E-02	1.870E-01	3.718E-02	1.858E-02	3.495E-02
	Thermal	0.000E+00	7.765E-01	0.000E+00	3.964E-02	0.000E+00	1.754E-01
2	Fast	1.278E-01	3.091E-02	6.271E-01	5.346E-02	1.284E-01	3.083E-02
	Thermal	0.000E+00	1.317E-01	1.729E-06	7.290E-01	0.000E+00	1.318E-01
3	Fast	1.865E-02	3.484E-02	1.871E-01	3.713E-02	6.200E-01	9.984E-02
	Thermal	0.000E+00	1.760E-01	0.000E+00	3.946E-02	3.660E-07	7.759E-01

Table A4: Response function of the coarse mesh in the inner reflector, in terms of surface and node averaged fluxes

Incoming surface	Group	Surface-averaged flux at outgoing surfaces						Node-averaged flux	
		1		2		3			
		Fast	Thermal	Fast	Thermal	Fast	Thermal	Fast	Thermal
1	Fast	3.310E+00	1.823E-01	3.607E-01	6.441E-02	3.171E-02	6.074E-02	1.859E+01	9.962E+00
	Thermal	0.000E+00	3.605E+00	0.000E+00	7.171E-02	0.000E+00	3.075E-01	2.489E-06	2.513E+01
2	Fast	2.371E-01	5.411E-02	3.293E+00	9.738E-02	2.388E-01	5.373E-02	2.053E+01	6.425E+00
	Thermal	0.000E+00	2.399E-01	4.673E-06	3.541E+00	0.000E+00	2.401E-01	2.572E-05	2.450E+01
3	Fast	3.184E-02	6.049E-02	3.606E-01	6.512E-02	3.310E+00	1.816E-01	1.859E+01	9.965E+00
	Thermal	0.000E+00	3.083E-01	0.000E+00	7.051E-02	2.952E-06	3.602E+00	2.541E-06	2.514E+01

Table A5: Relative errors of the superposition method as compared to the reference solutions – exiting currents for the coarse mesh in the outer reflector

Surface	1	2	3	4
Fast	0.030%	1.285%*	0.018%	0.001%
Thermal	0.028%	0.271%	0.058%	0.021%

*The uncertainty of the reference solution is about 1%.

Table A6: Relative errors of the superposition method as compared to the reference solutions –surface and node averaged fluxes for the coarse mesh in the outer reflector

	Surface averaged flux				Node averaged
Surface	1	2	3	4	
Fast	0.010%	1.66%*	0.006%	0.267%	0.075%
Thermal	0.030%	0.343%	0.013%	0.087%	0.083%

*The uncertainty of the reference solution is about 1%.

Table A7: Relative errors of the superposition method as compared to the reference solutions – exiting currents for the coarse mesh in the inner reflector

Surface	1	2	3
Fast	0.130%	0.024%	0.072%
Thermal	0.050%	0.054%	0.064%

Table A8: Relative errors of the superposition method as compared to the reference solutions – surface and node averaged fluxes for the coarse mesh in the inner reflector

	Surface averaged flux			Node averaged
Surface	1	2	3	
Fast	0.081%	0.184%	0.084%	0.141%
Thermal	0.017%	0.113%	0.066%	0.057%

Table A9: Ratios of incoming/outgoing partial currents for nodes 1-9

		Jin/Jout	
Node #	Surface	g=1	g=2
1	Left	1.000000E+00	1.000000E+00
	Right	1.473009E+00	1.035422E+00
2	Left	6.788823E-01	9.657901E-01
	Right	1.317759E+00	8.604942E-01
3	Left	7.588642E-01	1.162123E+00
	Right	1.037572E+00	9.252947E-01
4	Left	9.637890E-01	1.080737E+00
	Right	9.698727E-01	9.448198E-01
5	Left	1.031063E+00	1.058403E+00
	Right	9.224022E-01	9.394317E-01
6	Left	1.084126E+00	1.064473E+00
	Right	8.473549E-01	9.370870E-01
7	Left	1.180143E+00	1.067137E+00
	Right	5.693668E-01	1.005693E+00
8	Left	1.756337E+00	9.943396E-01
	Right	7.000748E-01	9.035756E-01
9	Left	1.428419E+00	1.106714E+00
	Right	0.000000E+00	0.000000E+00

Table A10: Two-group cross sections for nodes 1-9

Cross sections (cm**-1)										
		Node 1	Node 2	Node 3	Node 4	Node 5	Node 6	Node 7	Node 8	Node 9
Diffusion Coeff.	Group 1	8.550E-01	9.089E-01	1.672E+00	1.622E+00	1.610E+00	1.611E+00	1.633E+00	9.234E-01	8.707E-01
	Group 2	5.137E-01	6.299E-01	1.118E+00	1.132E+00	1.137E+00	1.136E+00	1.125E+00	6.504E-01	6.265E-01
Removal	Group 1	1.498E-05	5.272E-03	1.832E-03	2.373E-03	2.534E-03	2.540E-03	2.323E-03	4.679E-03	8.290E-03
	Group 2	2.647E-04	2.455E-04	4.648E-03	4.299E-03	4.181E-03	4.199E-03	4.452E-03	7.440E-04	2.445E-04
Nu·Fission	Group 1	0.000E+00	0.000E+00	2.889E-04	3.349E-04	3.479E-04	3.482E-04	3.302E-04	0.000E+00	0.000E+00
	Group 2	0.000E+00	0.000E+00	9.015E-03	8.325E-03	8.094E-03	8.129E-03	8.628E-03	0.000E+00	0.000E+00
Transfer 1->2		0.000E+00	5.263E-03	1.113E-03	1.500E-03	1.618E-03	1.622E-03	1.468E-03	4.657E-03	8.281E-03
Absorption	Group 1	1.498E-05	8.552E-06	7.187E-04	8.726E-04	9.159E-04	9.180E-04	8.550E-04	2.174E-05	9.700E-06
	Group 2	2.647E-04	2.455E-04	4.648E-03	4.299E-03	4.181E-03	4.199E-03	4.452E-03	7.440E-04	2.445E-04
Fission	Group 1	0.000E+00	0.000E+00	1.177E-04	1.368E-04	1.422E-04	1.423E-04	1.348E-04	0.000E+00	0.000E+00
	Group 2	0.000E+00	0.000E+00	3.707E-03	3.423E-03	3.328E-03	3.343E-03	3.548E-03	0.000E+00	0.000E+00
Total	Group 1	3.899E-01	3.667E-01	1.994E-01	2.055E-01	2.070E-01	2.069E-01	2.041E-01	3.610E-01	3.828E-01
	Group 2	6.489E-01	5.292E-01	2.982E-01	2.944E-01	2.933E-01	2.934E-01	2.962E-01	5.125E-01	5.321E-01
Discontinuity Factors	Left G1	7.499E-02	4.747E-02	7.782E-01	9.808E-01	1.069E+00	1.160E+00	1.378E+00	2.249E+00	2.820E+00
	Left G2	8.746E-01	8.445E-01	1.237E+00	1.128E+00	1.108E+00	1.125E+00	1.110E+00	9.866E-01	1.817E+00
	Right G1	5.098E+00	3.783E+00	1.125E+00	9.800E-01	9.066E-01	8.163E-01	5.785E-01	2.851E-01	6.378E-02
	Right G2	1.253E+00	7.330E-01	8.457E-01	8.966E-01	8.952E-01	8.832E-01	9.416E-01	8.366E-01	9.728E-02

FINAL REPORT

for

July 18, 2006 – July 31, 2007

of

Hybrid Coarse Mesh Transport/Diffusion Method for PBR Neutronics Analysis

Submitted by

Farzad Rahnema (PI) and Dingkang Zhang

Georgia Institute of Technology

in Collaboration with
Idaho National Laboratory

July 30, 2007

Summary

The objective of this project is to develop a method to generate transport theory response functions for non-multiplying regions in cylindrical geometry typical of pebble bed reactors (PBRs). This was accomplished in the three numerical steps. In the first step, the predefined phase space distribution of neutron particles on the boundary of a coarse mesh was first expanded as a multi-product of a set of orthogonal basis functions. In the second step, response functions for each cylindrical coarse mesh were generated by solving each local fixed source problem with the boundary condition imposed on one of the bounding surfaces. In the last step, a consistency check was performed to verify its accuracy.

In this project, the response expansion method was implemented into the MCNP code to calculate the response functions for coarse meshes in the inner and outer reflectors. The results obtained as a superposition of response functions were compared with the continuous energy Monte Carlo reference calculations. The excellent agreement between the two calculations indicates that the response functions can reproduce the reference solutions.

I. Introduction

The current generation of core neutronics methods for an analysis of the pebble bed reactor (PBR) is based on nodal diffusion theory and utilizes homogenized cross sections and other physics data generated by single assembly, infinite medium transport theory calculations. One of the primary limitations of nodal diffusion theory is its inadequacy to treat regions in the vicinity of strong neutron absorbers. A prime example of this shortcoming is the controlled reflector region in PBRs. These regions with no neutron multiplication and strong absorption do not receive satisfactory treatment in the nodal diffusion model. The goal of this project is to develop a method to generate the response functions for these regions. The response functions can be accommodated into the nodal diffusion equation to provide a transport solution for regions where the diffusion approximation is not sufficient.

The project consists of two phases. Phase I contains the development of 2-D work. Phase II was originally planed to further extend the method to 3-D. Because of funding unavailability, phase II has not been funded by INL. However, as requested by INL, we have generated homogenized cross sections for a simplified 1D slab PRB problem in phase II.

This final report is divided into four major sections. Section II contains an overview summarizing the objectives and work scope. Section III contains a complete description of the work performed in this project. Finally, Section IV highlights the project accomplishments.

II. Project Overview

Objective

The objective of this project is to develop a method to generate transport theory response functions for non-multiplying regions in 2-D cylindrical geometry typical of pebble bed reactors (PBRs). The method is to be implemented into the MCNP code to obtain a local transport solution for each unique coarse mesh in the outer or inner region as a response to incoming neutrons impinging on one of the bounding surfaces.

Work Scope

The main scope of work involves the development of expansion functions in 2D cylindrical geometry, the implementation of the new expansion functions into the MCNP code, the generation of response functions for non-multiplying regions, the consistency check to show the accuracy of the response functions, and generation of homogenized cross sections for a simplified 1-D slab PBR problem. The project consists of two phases. The phase I effort was focused on generation of the response functions for coarse meshes in the inner or outer reflector. The phase II effort was focused on generation of homogenized cross sections to account for intra-nodal leakages.

III. Technical Narrative

Task 1 Extend the method of calculating coarse mesh response functions from 1-D slab geometry to 2-D cylindrical geometry

Task Summary

The aim of this task was to extend the method of calculating the response functions from 1-D coarse meshes to 2-D cylindrical coarse meshes in both inner and outer reflectors. The main requirement is that this method can provide the response functions, in terms of node-averaged flux, surface-averaged flux and outgoing partial currents, corresponding to the incoming flux entering from one of the bounding surfaces.

Work Performed

The coarse-mesh methodology for the transport treatment of a set of selected nodes has been tailored to match the requirements of the CMFD method developed by INL and described in the proposal. INL method integrates the response matrices for the nodes necessitating transport treatment transparently in its formulation. As a result, Georgia Tech provides INL with response matrices that contain node responses to unit incoming partial currents, both in terms of node surface fluxes and node partial outgoing currents. The latter are needed to couple the transport-treated node to its neighbors.

Figure 1 illustrates the schematic configuration of a 2D PBMR400 pebble bed reactor, consisting of an inner reflector region, an annular fuel region and a controlled outer reflector. Let's begin with dividing both the outer and inner reflectors into a number of coarse meshes. The response functions of the coarse mesh corresponding to an incoming current from one of the adjacent regions can be calculated by solving the local problem below.

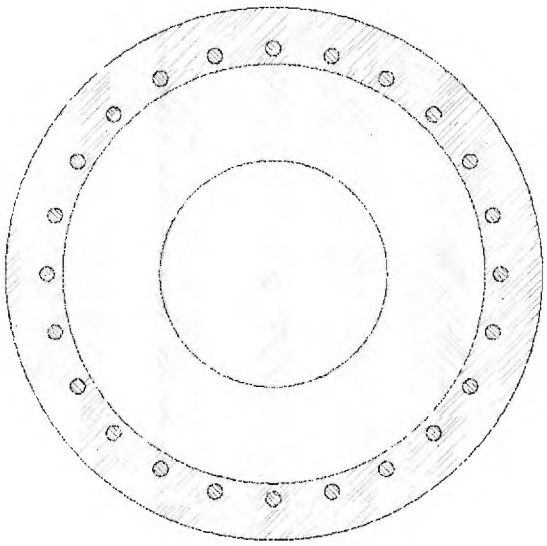

Fig. 1: 2-D simplified PBMR400 model

$$\frac{\mu}{r}\frac{\partial}{\partial r}\left(r\psi_i\left(r,\theta,\hat{\Omega},E\right)\right)+\frac{\eta}{r}\frac{\partial}{\partial\theta}\psi_i\left(r,\theta,\hat{\Omega},E\right)-\frac{1}{r}\frac{\partial}{\partial\omega}\left(\eta\psi_i\left(r,\theta,\hat{\Omega},E\right)\right)$$
$$+\sigma_i\left(r,\theta,E\right)\psi_i\left(r,\theta,\hat{\Omega},E\right)=Q_i\left(r,\theta,\hat{\Omega},E\right)+\int_0^\infty dE'\int_{4\pi}d\Omega'\ \sigma_s\left(r,\theta,\hat{\Omega}',E'\to\hat{\Omega},E\right)\psi_i\left(r,\theta,\hat{\Omega}',E'\right) \quad (1)$$

with the following boundary condition

$$\psi_i^-\left(r_{ij},\theta_{ij},\hat{\Omega},E\right)=\psi_j^+\left(r_{ij},\theta_{ij},\hat{\Omega},E\right) \text{ where } (r_{ij},\theta_{ij})\in\left\{V_i\cap V_j\right\} \text{ for all } V_j \text{ bounding } V_i \qquad (2)$$

In the above equations, $\psi_i\left(r,\theta,\hat{\Omega},E\right)$ is the neutron angular flux within coarse mesh i, r and θ are spatial variables in the cylindrical coordinate, ω and ξ are angular variables. Q is the internal volumetric source that may also include scattering neutrons. V_i represents all the sub-volume elements (i.e. coarse meshes). The superscripts "+" and "-"on the angular flux indicate the outgoing and incoming direction, respectively.

The MCNP code has been adapted to yield the solution to the local problem of Eq. (1). In the source-sampling subroutine, the initial position, direction and energy of source neutrons are sampled based on the predefined phase-space distribution on the boundary of a coarse mesh. If $f(r,\theta,\hat{\Omega},E)$ is the predefined distribution function, the initial position, energy and direction of incoming neutrons are sampled from the following distribution.

$$\Gamma_{ij}^-(w_{is}^-)=f\left(r,\theta,\hat{\Omega},E\right) \qquad (3)$$

In the tally subroutine, the expected value of response functions, in terms of the node-average flux, surface-averaged flux and partial currents crossing a coarse mesh, are tallied as the probability that initial neutrons and their progenies escape from the coarse mesh through a specific surface, scaled by a weight factor determined by the orders of the expansion and the location, energy and direction of the exiting neutrons.

$$RJ(k)_{i,j'\to j}^{n'\to n}=\frac{1}{NA_{ij}^n}\sum_{c=1}^{N}f_{ij}^{+,n}\left(\vec{r}_c,E_c,\hat{\Omega}_c\right)w_c \qquad (4)$$

where $\vec{r}_c,E_c,\hat{\Omega}_c$ and w_c are the position, energy, direction and weight of the exiting neutrons, and $f_{ij}^{+,n}\left(\vec{r}_c,E_c,\hat{\Omega}_c\right)$ are the expansion functions.

The code was tested by comparisons with results from direct MCNP simulations on 2-D benchmark problems. A consistency check to further verify the accuracy of the response functions, based on comparisons of the superposition of response functions and MCNP solutions, was performed upon the completion of task 2.

Task 2 Development of 2D cylindrical expansion functions

Task Summary

The aim of this task was to develop an expansion scheme to approximate the angular flux on a coarse mesh interface in 2D cylindrical geometry. The idea behind expansion functions is the development of the boundary condition imposed on the node boundary as an expansion of an orthogonal set of basis functions in space, energy and angle. The basis functions are selected so that a relatively low order truncation would lead to accurate solutions inside the node. The Monte Carlo code MCNP allows surface-source boundary conditions in terms of isotropic and cosine angular distributions and uniform and linear spatial distribution. Higher orders of expansion would require a modification to the MCNP source code. The expansion approximation should guarantee conservation of particle and be able to provide the scalar flux at the incident surface.

Work Performed

(1) Expansion functions

Following Mosher and Rahnema (2006)[1] and Forget and Rahnema (2007)[2], one may expand the angular current at each interface in terms of Legendre polynomials as in Eq. (5). This is a natural choice, since the 0^{th} order expansion in angle corresponds to an isotropic surface source, and the 0^{th} order expansion in space corresponds to a uniform source. However, this expansion scheme cannot be applied to cylindrical geometry as in this project, since an isotropic angular current (i.e. angular flux $\Psi = 1/\mu$), leads to an infinite scalar flux on the incident surface.

$$J(x,\mu,\phi,E) = \sum_{i,j,k,l} J_{ijkl} P_i(x) P_j(\mu) P_k(\phi) P_l(E) \tag{5}$$

To accomplish the goals of this task, we choose to expand the angular flux, instead of angular current, at each surface in terms of a set of expansion (basis) functions.

$$\psi(x,\hat{\Omega},E) = \sum_{i,j,k,l} c_{ijkl} f_{ijkl}(x,\hat{\Omega},E) \tag{6}$$

In the above equation, c_{ijkl} are expansion coefficients, and $f_{ijkl}(x,\hat{\Omega},E)$ represent expansion functions. However, in order to ensure that the total number of particles (or current) is conserved, the expansion functions must be constructed to have the following orthogonality.

$$\int dx \int dE \int_{\vec{n}\cdot\hat{\Omega}>0} d\hat{\Omega}(\vec{n}\cdot\hat{\Omega}) f_{ijkl}(x,\hat{\Omega},E) f_{i'j'k'l'}(x,\hat{\Omega},E) = A_{ijkl}\delta_{ii'}\delta_{jj'}\delta_{kk'}\delta_{ll'} \tag{7}$$

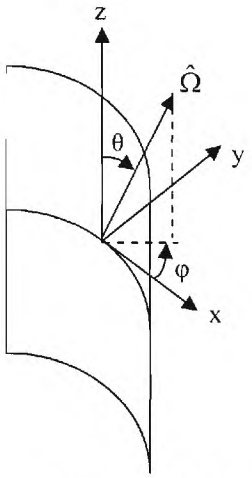

Fig. 2: Angular variables in a 2D cylindrical surface

As an example, take a 2D cylindrical surface shown in Fig. 2 in which axis z is chosen to be parallel with the axis of the cylinder and y represents the normal direction at point $\vec{r}$. In this case, the expansion functions can be written as in the following form[3].

---

[1] Scott Mosher and F. Rahnema, "The Incident Flux Response Expansion Method for Heterogeneous Coarse Mesh Transport Problems," *Transport Theory and Statistical Physics*, **34**, No. 6, 1-26 (2006).

[2] Benoit Forget and Farzad Rahnema, "Hybrid Coarse Mesh Radiation Transport Method for Whole Core Reactor Criticality Analysis," *Nucl. Sci. Eng.*, Submitted (December 2006).

[3] Dingkang Zhang, Farzad Rahnema, and Abderrafi M Ougouag, "New Expansion Functions for Calculation of Coarse Mesh Response Functions", the 2007 ANS Annual Meeting, Boston, MA, June 24-28, 2007

$$f_{ijkl}\left(x,\hat{\Omega},E\right)=\overline{P}_i\left[x_{\min},x_{\max}\right](x)U_j\left(\cos\theta\right)P_j\left(\cos\phi\right)\overline{P}_l\left[E_{g-1},E_g\right](E) \tag{8}$$

where scaled Legendre polynomials $\overline{P}_i\left[x_{\min},x_{\max}\right](x)$ and Chebyshev polynomials of the second kind $U_j(x)$ are defined as:

$$\overline{P}_i\left[x_{\min},x_{\max}\right](x)=P_i\left(\frac{2(x-x_{\min})}{x_{\max}-x_{\min}}-1\right) \tag{9}$$

and

$$\begin{aligned} U_0(x)&=1 \\ U_1(x)&=2x \\ U_n(x)&=2xU_{n-1}(x)-U_{n-2}(x) \quad \text{for } n\geq 2 \end{aligned} \tag{10}$$

(2) Consistency check

The method and expansion functions developed in tasks 1 and 2 have been successfully implemented into the MCNP code. Generation of response functions consists of two steps. In the first step, the MCNP code was used to compute a reference solution, and the actual neutron spatial, energy and angular distributions were tallied and expanded in terms of the expansion functions constructed in this research. In the second step, the response functions of a coarse mesh associated with the incoming neutron flux at each bounding surface were generated.

To verify the validity of the method, a 2D cylindrical benchmark problem shown in Fig. 3 was considered. The 2-D benchmark consists of an inner reflector region with a diameter of 2 meters (m), an annular fuel region of 0.85 m thickness and a 0.5 m thick controlled outer reflector region. There are 24 control rods each of 13 cm diameter whose centers are positioned on the circumference of 3.974 m diameter ring. The material compositions are listed in Table 1.

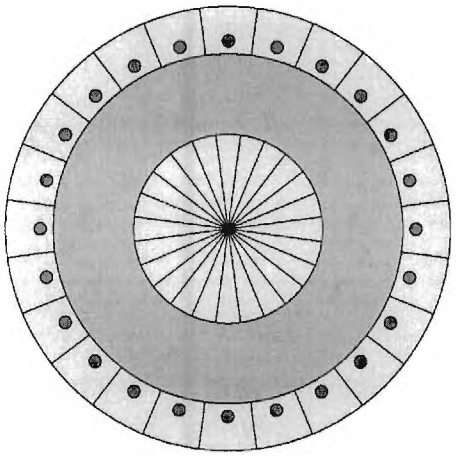

Fig. 3: Geometric configuration of a 2D cylindrical benchmark problem

Table 1 Material composition in each region

Region	Material	Atomic Density (10^{-24})
Inner Reflector	C	1.18234E-01
	U234	1.16811E-07
	U235	1.19359E-05

Fuel	U238	1.10859E-04
	Xe135	3.43000E-11
	O16	2.45830E-04
	Si	2.75487E-04
	Ni	1.04518E-04
	Cr	1.34381E-04
	Fe	5.07660E-04
	C	6.81785E-02
Outer Reflector	C	1.18894E-01
Control Rod	B10	3.20000E-06
	C	9.54760E-02

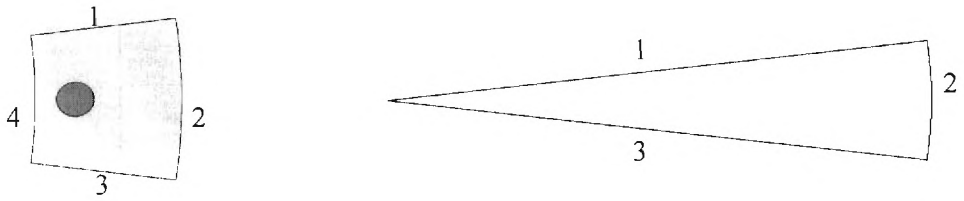

(a) coarse mesh in the outer reflector (b) coarse mesh in the inner reflector

Fig. 4: Configurations of coarse meshes

Both the outer and inner reflectors were divided into 24 coarse meshes. The geometrical configurations of these coarse meshes are shown in Figs. 4. The response functions, in terms of exiting partial currents, surface-averaged angular fluxes and node-averaged fluxes, are listed in Tables A1-A4.

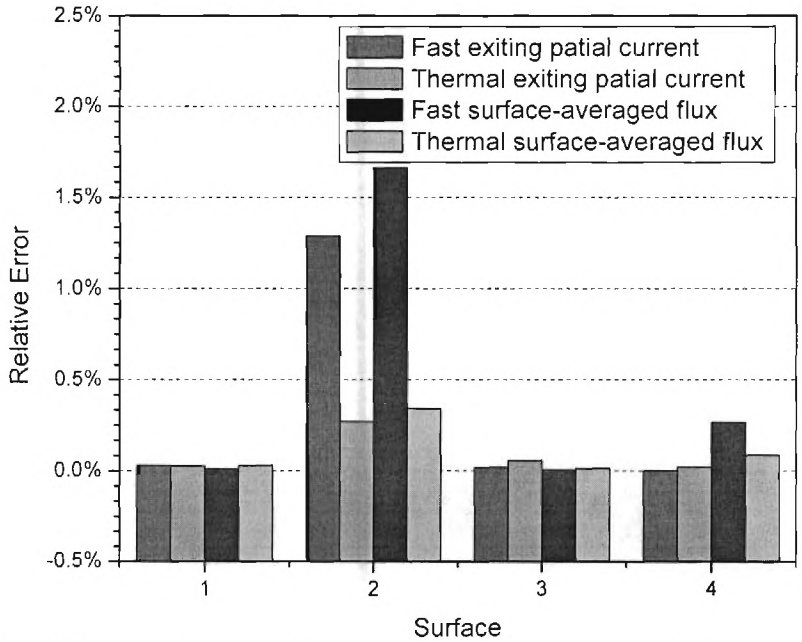

Fig. 5: Relative difference between the superposition based response functions and reference solutions for the outer reflector coarse mesh

To check the accuracy of these response functions, the superposition of these response functions was compared with the reference results computed from the continuous-energy MCNP simulations. The relative difference between the two solutions for the outer reflector coarse mesh is illustrated in Fig. 5. The detailed comparisons for both the inner and outer reflector coarse meshes are listed in Tables A5-A8. It can be found that the agreement between the two solutions is excellent. Most of the relative errors are less than 0.2%. The maximum relative difference of 1.6% occurs on the outer surface (surface 2 in Fig. 4) of the coarse mesh in the outer reflector where the uncertainty of the reference solution is about 1%; however it is still within the two standard deviations of the reference solutions. These results indicate that the response functions based on the method and expansion functions developed in this work are accurate and can reproduce solutions to the same level as continuous energy MCNP calculations.

Task 3 Generation of homogenized cross sections for a 1-D slab problem specified by INL

Task summary:

The aim of the task was to generate homogenized parameters (cross sections, discontinuity factors) for 1-D coarse meshes. Conventionally, the assumption of infinite media (i.e. specular reflection boundary condition) is used to calculate approximate spectrum for each coarse mesh (lattice cell) and then homogenized data are collapsed. To account for the intra-nodal leakage, the ratios of incoming/outgoing partial currents provided by INL were taken into account when we calculated the homogenized parameters.

Work performed

The problem is a 1-D adaptation of a realistic 2-D model of the PBMR400 pebble bed reactor shown in Fig. 3. The specifications for the 2-D model are based on data provided by INL and are representative of an equilibrium core. The 1-D benchmark is a section of the 2-D configuration taken along a semi-plane perpendicular to the paper and passing through the centers of the reactor and of one of the control rods. Its geometrical layout and its subdivision into nodes are illustrated in Figure 6. Reflective and vacuum boundary conditions were imposed on the left and right boundary of the system, respectively. The width of each region was taken to be the same as the corresponding radial width of the 2-D region. Material densities in each region are listed in Table 2. The ratios of incoming/outgoing partial currents provided by INL are illustrated in Table A9 in Appendix

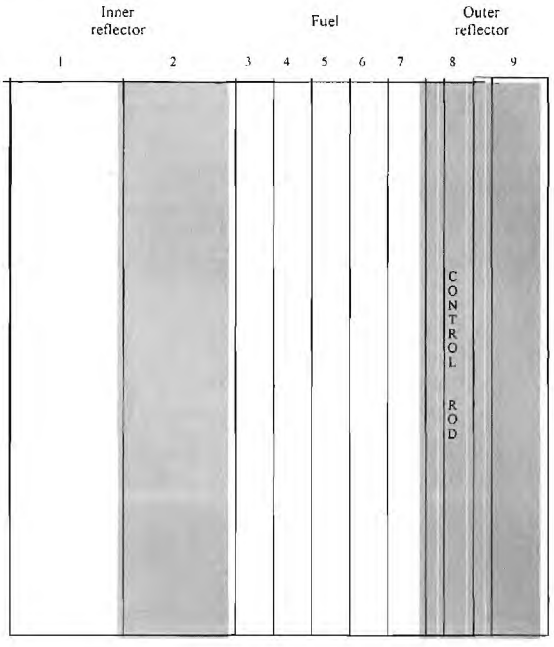

Fig. 6: 1-D simplified PBMR400 models

Table 2: Material compositions in each region (unit: 10E24 atoms/cm^{-3})

Elements	Inner reflector	Fuel	Outer reflector	Control Rod
C	1.18234E-01	6.81785E-02	1.18894E-01	9.54760E-02
U-234		1.16811E-07		
U-235		1.19359E-05		
U-238		1.10859E-04		
Xe-135		3.43000E-11		
O		2.45830E-04		
Si		2.75487E-04		
Ni		1.04518E-04		
Cr		1.34381E-04		
Fe		5.07660E-04		
B				3.20000E-06

A continuous energy Monte Carlo calculation was performed to calculate the neutron angular flux $\psi(z,\mu,E)$ within each coarse mesh. To preserve various reaction rates, the homogenized multi-group cross section were computed by the following equations:

$$\sigma_g = \frac{\int_V dz \int_{E_{g-1}}^{E_g} dE \int_{-1}^{1} d\mu \psi(z,\mu,E)\sigma(z,E)}{\int_V dz \int_{E_{g-1}}^{E_g} dE \int_{-1}^{1} d\mu \psi(z,\mu,E)}$$

$$\sigma_{a,g} = \frac{\int_V dz \int_{E_{g-1}}^{E_g} dE \int_{-1}^{1} d\mu \psi(z,\mu,E)\sigma_a(z,E)}{\int_V dz \int_{E_{g-1}}^{E_g} dE \int_{-1}^{1} d\mu \psi(z,\mu,E)}$$

$$\sigma_{f,g} = \frac{\int_V dz \int_{E_{g-1}}^{E_g} dE \int_{-1}^{1} d\mu \psi(z,\mu,E)\sigma_f(z,E)}{\int_V dz \int_{E_{g-1}}^{E_g} dE \int_{-1}^{1} d\mu \psi(z,\mu,E)}$$

$$\nu\sigma_{f,g} = \frac{\int_V dz \int_{E_{g-1}}^{E_g} dE \int_{-1}^{1} d\mu \psi(z,\mu,E)\nu\sigma_f(z,E)}{\int_V dz \int_{E_{g-1}}^{E_g} dE \int_{-1}^{1} d\mu \psi(z,\mu,E)}$$

$$\sigma_s^{g'g} = \frac{\int_V dz \int_{E_{g-1}}^{E_g} dE \int_{E_{g'-1}}^{E_{g'}} dE' \int_{-1}^{1} d\mu' \int_{-1}^{1} d\mu \psi(z,\mu',E') \nu\sigma_s(z,E' \to E,\mu_0)}{\int_V dz \int_{E_{g-1}}^{E_g} dE \int_{-1}^{1} d\mu \psi(z,\mu,E)}$$

Table A10 shows the MCNP collapsed two-group cross sections as well as discontinuity factors for nodes 1-9.

IV. Summary and Conclusions

Milestone/Task Description	Planned Completion Date	Actual Completion Date	Percent Complete
Task 1: 2D extension	October 17, 2006	October 17, 2006	100%
Task 2: 2D representation functions	December 17, 2006	December 17, 2006	100%
Task 3: Cross section generation	June 30, 2007	June 30, 2007	100%

We have successfully extended the method of calculating coarse mesh response functions from 1D slab to 2D cylindrical geometry. A set of new expansion functions, has been developed and implemented into the MCNP code. Unlike the Legendre expansion functions, the new expansion set avoids scalar flux singularity on the incident surface and at the same time ensures conservation of particles, i.e. the total current crossing an interface remains unchanged after expansion. A consistency check has been performed to demonstrate the accuracy of the method and the expansion functions. In addition, the MCNP code has been used to generate the homogenized parameters for the simplified 1-D PBR problem to account for intra-nodal leakages.

IV. APPENDIX:

Table A1: Response function of the coarse mesh in the outer reflector, in terms of exiting currents

Incoming surface	Group	Exiting Currents at outgoing surfaces							
		1		2		3		4	
		Fast	Thermal	Fast	Thermal	Fast	Thermal	Fast	Thermal
1	Fast	6.166E-01	1.086E-01	1.836E-03	1.297E-02	1.988E-04	5.156E-03	1.896E-01	4.813E-02
	Thermal	6.645E-07	8.251E-01	0.000E+00	3.513E-02	0.000E+00	5.127E-03	1.920E-07	1.051E-01
2	Fast	0.000E+00	0.000E+00	0.000E+00	0.000E+00	0.000E+00	0.000E+00	0.000E+00	0.000E+00
	Thermal	0.000E+00	0.000E+00	0.000E+00	0.000E+00	0.000E+00	0.000E+00	0.000E+00	0.000E+00
3	Fast	1.949E-04	5.166E-03	1.840E-03	1.296E-02	6.165E-01	1.087E-01	1.896E-01	4.815E-02
	Thermal	0.000E+00	5.128E-03	0.000E+00	3.516E-02	6.778E-07	8.251E-01	1.131E-07	1.051E-01
4	Fast	6.605E-02	3.002E-02	9.495E-04	1.382E-02	6.604E-02	3.001E-02	6.733E-01	9.294E-02
	Thermal	3.491E-07	7.713E-02	0.000E+00	8.394E-03	2.659E-07	7.710E-02	1.909E-06	7.921E-01

Table A2: Response function of the coarse mesh in the outer reflector, in terms of surface and node averaged fluxes

Incoming surface	Group	Surface-averaged flux at outgoing surfaces								Node-averaged flux	
		1		2		3		4			
		Fast	Thermal	Fast	Thermal	Fast	Thermal	Fast	Thermal	Fast	Thermal
1	Fast	3.309E+00	1.973E-01	3.156E-03	2.246E-02	3.408E-04	8.929E-03	3.680E-01	8.424E-02	1.979E+01	2.178E+01
	Thermal	2.132E-06	3.686E+00	0.000E+00	6.092E-02	0.000E+00	8.830E-03	2.957E-07	1.911E-01	1.361E-05	4.636E+01
2	Fast	0.000E+00	0.000E+00	0.000E+00	0.000E+00	0.000E+00	0.000E+00	0.000E+00	0.000E+00	0.000E+00	0.000E+00
	Thermal	0.000E+00	0.000E+00	0.000E+00	0.000E+00	0.000E+00	0.000E+00	0.000E+00	0.000E+00	0.000E+00	0.000E+00
3	Fast	3.289E-04	8.967E-03	3.150E-03	2.242E-02	3.309E+00	1.974E-01	3.680E-01	8.429E-02	1.976E+01	2.176E+01
	Thermal	0.000E+00	8.839E-03	0.000E+00	6.107E-02	2.723E-06	3.685E+00	1.349E-07	1.909E-01	1.294E-05	4.637E+01
4	Fast	1.234E-01	5.217E-02	1.609E-03	2.397E-02	1.232E-01	5.226E-02	3.365E+00	1.672E-01	2.856E+01	2.684E+01
	Thermal	9.444E-07	1.402E-01	0.000E+00	1.446E-02	3.912E-07	1.404E-01	7.587E-06	3.644E+00	4.370E-05	4.227E+01

Table A3: Response function of the coarse mesh in the inner reflector, in terms of exiting currents

Incoming surface	Group	Exiting Currents at outgoing surfaces					
		1		2		3	
		Fast	Thermal	Fast	Thermal	Fast	Thermal
1	Fast	6.202E-01	9.987E-02	1.870E-01	3.718E-02	1.858E-02	3.495E-02
	Thermal	0.000E+00	7.765E-01	0.000E+00	3.964E-02	0.000E+00	1.754E-01
2	Fast	1.278E-01	3.091E-02	6.271E-01	5.346E-02	1.284E-01	3.083E-02
	Thermal	0.000E+00	1.317E-01	1.729E-06	7.290E-01	0.000E+00	1.318E-01
3	Fast	1.865E-02	3.484E-02	1.871E-01	3.713E-02	6.200E-01	9.984E-02
	Thermal	0.000E+00	1.760E-01	0.000E+00	3.946E-02	3.660E-07	7.759E-01

Table A4: Response function of the coarse mesh in the inner reflector, in terms of surface and node averaged fluxes

Incoming surface	Group	Surface-averaged flux at outgoing surfaces						Node-averaged flux	
		1		2		3			
		Fast	Thermal	Fast	Thermal	Fast	Thermal	Fast	Thermal
1	Fast	3.310E+00	1.823E-01	3.607E-01	6.441E-02	3.171E-02	6.074E-02	1.859E+01	9.962E+00
	Thermal	0.000E+00	3.605E+00	0.000E+00	7.171E-02	0.000E+00	3.075E-01	2.489E-06	2.513E+01
2	Fast	2.371E-01	5.411E-02	3.293E+00	9.738E-02	2.388E-01	5.373E-02	2.053E+01	6.425E+00
	Thermal	0.000E+00	2.399E-01	4.673E-06	3.541E+00	0.000E+00	2.401E-01	2.572E-05	2.450E+01
3	Fast	3.184E-02	6.049E-02	3.606E-01	6.512E-02	3.310E+00	1.816E-01	1.859E+01	9.965E+00
	Thermal	0.000E+00	3.083E-01	0.000E+00	7.051E-02	2.952E-06	3.602E+00	2.541E-06	2.514E+01

Table A5: Relative errors of the superposition method as compared to the reference solutions – exiting currents for the coarse mesh in the outer reflector

Surface	1	2	3	4
Fast	0.030%	1.285%*	0.018%	0.001%
Thermal	0.028%	0.271%	0.058%	0.021%

*The uncertainty of the reference solution is about 1%.

Table A6: Relative errors of the superposition method as compared to the reference solutions –surface and node averaged fluxes for the coarse mesh in the outer reflector

	Surface averaged flux				Node averaged
Surface	1	2	3	4	
Fast	0.010%	1.66%*	0.006%	0.267%	0.075%
Thermal	0.030%	0.343%	0.013%	0.087%	0.083%

*The uncertainty of the reference solution is about 1%.

Table A7: Relative errors of the superposition method as compared to the reference solutions – exiting currents for the coarse mesh in the inner reflector

Surface	1	2	3
Fast	0.130%	0.024%	0.072%
Thermal	0.050%	0.054%	0.064%

Table A8: Relative errors of the superposition method as compared to the reference solutions – surface and node averaged fluxes for the coarse mesh in the inner reflector

	Surface averaged flux			Node averaged
Surface	1	2	3	
Fast	0.081%	0.184%	0.084%	0.141%
Thermal	0.017%	0.113%	0.066%	0.057%

Table A9: Ratios of incoming/outgoing partial currents for nodes 1-9

		Jin/Jout	
Node #	Surface	g=1	g=2
1	Left	1.000000E+00	1.000000E+00
	Right	1.473009E+00	1.035422E+00
2	Left	6.788823E-01	9.657901E-01
	Right	1.317759E+00	8.604942E-01
3	Left	7.588642E-01	1.162123E+00
	Right	1.037572E+00	9.252947E-01
4	Left	9.637890E-01	1.080737E+00
	Right	9.698727E-01	9.448198E-01
5	Left	1.031063E+00	1.058403E+00
	Right	9.224022E-01	9.394317E-01
6	Left	1.084126E+00	1.064473E+00
	Right	8.473549E-01	9.370870E-01
7	Left	1.180143E+00	1.067137E+00
	Right	5.693668E-01	1.005693E+00
8	Left	1.756337E+00	9.943396E-01
	Right	7.000748E-01	9.035756E-01
9	Left	1.428419E+00	1.106714E+00
	Right	0.000000E+00	0.000000E+00

Table A10: Two-group cross sections for nodes 1-9

Cross sections (cm**-1)										
		Node 1	Node 2	Node 3	Node 4	Node 5	Node 6	Node 7	Node 8	Node 9
Diffusion Coeff.	Group 1	8.550E-01	9.089E-01	1.672E+00	1.622E+00	1.610E+00	1.611E+00	1.633E+00	9.234E-01	8.707E-01
	Group 2	5.137E-01	6.299E-01	1.118E+00	1.132E+00	1.137E+00	1.136E+00	1.125E+00	6.504E-01	6.265E-01
Removal	Group 1	1.498E-05	5.272E-03	1.832E-03	2.373E-03	2.534E-03	2.540E-03	2.323E-03	4.679E-03	8.290E-03
	Group 2	2.647E-04	2.455E-04	4.648E-03	4.299E-03	4.181E-03	4.199E-03	4.452E-03	7.440E-04	2.445E-04
Nu·Fission	Group 1	0.000E+00	0.000E+00	2.889E-04	3.349E-04	3.479E-04	3.482E-04	3.302E-04	0.000E+00	0.000E+00
	Group 2	0.000E+00	0.000E+00	9.015E-03	8.325E-03	8.094E-03	8.129E-03	8.628E-03	0.000E+00	0.000E+00
Transfer 1->2		0.000E+00	5.263E-03	1.113E-03	1.500E-03	1.618E-03	1.622E-03	1.468E-03	4.657E-03	8.281E-03
Absorption	Group 1	1.498E-05	8.552E-06	7.187E-04	8.726E-04	9.159E-04	9.180E-04	8.550E-04	2.174E-05	9.700E-06
	Group 2	2.647E-04	2.455E-04	4.648E-03	4.299E-03	4.181E-03	4.199E-03	4.452E-03	7.440E-04	2.445E-04
Fission	Group 1	0.000E+00	0.000E+00	1.177E-04	1.368E-04	1.422E-04	1.423E-04	1.348E-04	0.000E+00	0.000E+00
	Group 2	0.000E+00	0.000E+00	3.707E-03	3.423E-03	3.328E-03	3.343E-03	3.548E-03	0.000E+00	0.000E+00
Total	Group 1	3.899E-01	3.667E-01	1.994E-01	2.055E-01	2.070E-01	2.069E-01	2.041E-01	3.610E-01	3.828E-01
	Group 2	6.489E-01	5.292E-01	2.982E-01	2.944E-01	2.933E-01	2.934E-01	2.962E-01	5.125E-01	5.321E-01
Discontinuity Factors	Left G1	7.499E-02	4.747E-02	7.782E-01	9.808E-01	1.069E+00	1.160E+00	1.378E+00	2.249E+00	2.820E+00
	Left G2	8.746E-01	8.445E-01	1.237E+00	1.128E+00	1.108E+00	1.125E+00	1.110E+00	9.866E-01	1.817E+00
	Right G1	5.098E+00	3.783E+00	1.125E+00	9.800E-01	9.066E-01	8.163E-01	5.785E-01	2.851E-01	6.378E-02
	Right G2	1.253E+00	7.330E-01	8.457E-01	8.966E-01	8.952E-01	8.832E-01	9.416E-01	8.366E-01	9.728E-02